Numerical Simulation of Terrestrial Radiation over a Snow Cover

P. DUCHARME

Saint-Eustache, Quebec, Canada

A. HOUDAYER*

Laboratoire R.-J.-A.-Lévesque, Université de Montréal, Montreal, Quebec, Canada

Y. CHOQUETTE AND B. KAPFER

Institut de Recherche d'Hydro-Québec (IREQ), Varennes, Quebec, Canada

J. P. MARTIN

Laboratoire R.-J.-A.-Lévesque, Université de Montréal, Montreal, Quebec, Canada

(Manuscript received 8 May 2014, in final form 1 October 2014)

ABSTRACT

The intensity of terrestrial gamma radiation is a function of a number of parameters: emissivity and spatial distribution of the radioactive material in the soil, snow/water cover above ground, soil moisture content, type, and height above ground of the detector. Thus, the conversion of gamma measurements into reliable information must be based on a solid knowledge of the behavior of the gamma detector under different conditions. Such a detector, using a cylindrical NaI(Tl) crystal, was developed to remotely and automatically provide information on snow water equivalent (SWE) and soil moisture content (M). It became rapidly obvious that the behavior of the detector [gamma monitor (GMON)] over an infinite source could not be exactly reproduced in a laboratory. Therefore, a relatively simple model to simulate the behavior of GMON and to establish the relevant data analysis algorithms was conceived. This paper presents the basic assumptions for developing the model, the resulting algorithms, a comparison with field measurements, and some useful information on how GMON reacts to various field conditions.

1. Introduction

For decades now, scientists have estimated SWE and, to some extent, soil moisture content (M) by measuring the attenuation of natural soil gamma radiation through the snowpack (Carroll and Schaake 1983; Maxson et al. 1996; Grasty 1982). Airborne surveys of SWE are routinely conducted by NOAA's National Operational Hydrologic Remote Sensing Center using this technique. The basic concepts and data analysis algorithms used are described in detail by Fritzsche (1982).

Following the same path, Hydro-Québec and its partners have developed a remote and automatic version of this technology [gamma monitor (GMON); now commercialized by Campbell Scientific (Canada) Corp. under the name CS725] for permanent deployment at specific sites (Martin et al. 2008; Choquette et al. 2008). In this case, an NaI(Tl) detector is put atop a pole, normally at 2.5 m above ground. At first, laboratory tests were conducted with a GMON suspended over a tank filled with varying volumes of water with the objective of developing appropriate data analysis algorithms. But the resulting algorithms fail to deliver accurate SWE measurements (a margin of error of 5% or less) when the GMON is moved from the laboratory to a field station. For a given snowpack, the trajectories and therefore the attenuation ratios are larger for gammas

Denotes Open Access content.

* Deceased.

Corresponding author address: Y. Choquette, IREQ, 1800 Blvd. Lionel Boulet, Varennes QC J3X 1S1, Canada.
E-mail: choquette.yves@ireq.ca

DOI: 10.1175/JTECH-D-14-00100.1

coming from areas farther away from the detector. A limited size pool setup fails to reproduce this effect. The alternative of conducting field measurement campaigns at each GMON site in order to determine the appropriate data analysis algorithms was judged untimely and expensive. The number of parameters to monitor and control is large and so are the differences from site to site.

Therefore, we undertook the development of a numerical model to simulate the behavior of GMON under different conditions, so as to establish data analysis algorithms and to identify the reliability and limitations of the instrument. Besides the ability to transpose the measured signals in actual SWE values, we gained insights into a number of relevant questions: What is the expected accuracy of the SWE estimates? What is the size of the area covered? What is the effect of soil moisture on the signal? Does the height above ground of the GMON modify its response? Other questions, some of which are reported on below, are also discussed.

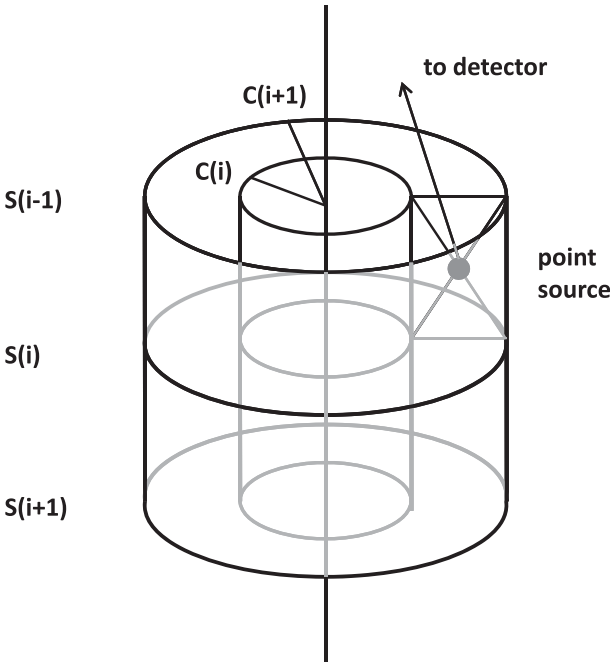

FIG. 1. Numerical description of the source in the model.

2. GMON and numerical model

The GMON is described in detail in the U.S. patent by Choquette et al. (2008). It is composed of a cylindrical 7.62 cm × 7.62 cm NaI(Tl) crystal coupled to a photomultiplier counter. Although we have simulated GMON at various heights above ground, in this document we will, unless stated otherwise, present results relative to a detector at 2.5 m. Based on climatology, that is the height at most of our GMON sites. The detector and the relevant electronics (data management, analysis, and communications) are inserted into a thin aluminum tubing that is itself inserted into a sealed aluminum-tube-shaped housing. The model neglects the thin tubing given its small thickness and the fact that it completely encloses the detector. The bottom surface of the external tubing is made of a 3-mm plate of aluminum to maximize the number of gammas reaching the crystal. A hollow lead or steel cylinder, called a collimator, may be fixed around the bottom portion of the aluminum cylinder as a partial shield, reducing the area being effectively monitored and filtering most of the gammas from the surrounding areas. CS725 is the actual commercial name for the collimated and noncollimated or unshielded versions of the sensor. We present here the results relevant to the unshielded CS725 model and the results from the corresponding numerical simulations.

The multichannel amplifier and the software in the CS725 target two specific windows of energy: one centered at 1.46 MeV and associated with the ^{40}K isotope, and one at 2.61 MeV, the ^{208}Tl isotope. These two isotopes are present in all types of soil, and they emit gammas with enough energy (1.46 and 2.61 MeV) to travel through significant layers of water and yet weak enough to be significantly attenuated by it. This qualifies them as useful indicators to measure SWE. The signal is stripped of the background noise to isolate the counts directly associated with these two isotopes and to filter out the contributions of other radioactive sources (Choquette et al. 2008). By stripping the signal, we isolate the monochromatic population of gammas at 1.46 and 2.61 MeV. The monochromatic nature of the resulting signal allows for the simulation of the attenuation through the various materials. Throughout the document we will present the figures and results corresponding to the 1.46-MeV window. Although the numbers are slightly different for the 2.61-MeV window, the overall conclusions are basically the same. Accordingly, the simulation model is based on the assumption of a monochromatic source.

The ground half-space, under the detector, is divided into C vertical concentric cylinders of depth D. Each cylinder, centered by the vertical axis passing through the detector, is itself divided in S layers (Fig. 1). As a result, the source is represented as CS annular sections. The thickness assigned to each cylinder varies, so as to favor a higher resolution for the areas under and close to the detector. Giving the symmetric nature of the system—source cylinders and cylindrical detector—each annular

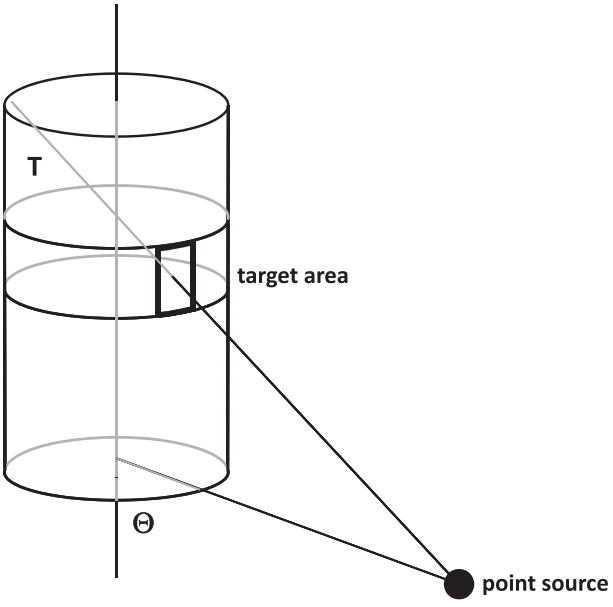

FIG. 2. Radiation from the source S sweeping the detector and associated trajectories T_i within the crystal.

section is handled as a point source, located halfway between the inner and outer surfaces of the annular volume source. The number of gamma rays emitted by the source by unit of time is derived from the density, the volume, and the emissivity of the substance within the source volume.

In the model, the surface of the NaI(Tl) crystal is marked out in n target areas (Fig. 2). In sequence, the model calculates the distance between each point source and the center of each target square. For each of these trajectories, the strength of the source signal is reduced to account for dilution with distance from the source and for the effective target area (orthogonal to the trajectory). The signal is also attenuated by the mass of soil on its trajectory; the soil water content; the snow/ice/water on the ground; the air; the collimator around the detector, if any; and the aluminum housing containing the NaI(Tl) crystal. The attenuation of the monochromatic gamma beam through each material is calculated using

$$I = I_o e^{(-\beta T)}, \tag{1}$$

where I is the gamma counts at the entrance of a volume of a given material, I_o is the gamma counts at the exit of the volume of material, T is the length of the trajectory in the material, and β is the linear total attenuation coefficient of the material.

TABLE 1. Mass attenuation coefficients for different materials and gamma energy levels.

Material	1.46 MeV ($cm^2\,g^{-1}$)	2.61 MeV ($cm^2\,g^{-1}$)
Aluminum	5.07×10^{-2}	3.38×10^{-2}
NaI	4.71×10^{-2}	3.38×10^{-2}
Water	5.85×10^{-2}	4.34×10^{-2}
Soil	5.27×10^{-2}	3.94×10^{-2}
Air	5.27×10^{-2}	3.94×10^{-2}

The linear coefficient of the monochromatic gammas is specific to each material and each energy level (National Institute of Standards and Technology 2013). Mass attenuation coefficients are provided in Table 1. These coefficients are multiplied by the density of the material to calculate the corresponding linear attenuation coefficients. Mass coefficients for soil and air are 0.9009 times the coefficient of water (Fritzsche 1982; Offenbacher and Colbeck 1991).

The density of air is derived from the World Meteorological Organization's definition of a standard atmosphere, and we neglect the contribution of water vapor in the column of air. We also neglect attenuation by the mass of air within the soil. These approximations introduce errors of less than a tenth of a millimeter of SWE—that is largely within the precision targets set for this technological innovation project.

The signal emitted from a volume source of soil, located at an angle θ with respect to the vertical axis of the crystal, is attenuated by soil, the soil water content, the SWE, and air according to the following equation:

$$I = I_o e^{\{-\mu_S \rho_S Z \sec(\theta) - \mu_W \rho_S M Z \sec(\theta) - \beta_W [\mathrm{SWE} + (H - \mathrm{SWE}) 0.001\,164] \sec(\theta)\}}, \tag{2}$$

where I is the nonattenuated portion of the signal at a distance from the source equal to the distance between the source and the target area on the CS725, I_o is the signal emitted by the volume source in all directions, μ_S is the mass attenuation coefficient of dry soil, ρ_S is the dry soil density, Z is the depth in the ground of the point source, μ_W is the mass attenuation coefficient of water, M is the ratio of the mass of water to the mass of dry soil by unit volume of soil, β_W is the linear attenuation coefficient of water, H is the height of the base of the CS725 above ground, and 0.001 164 is the ratio of the linear attenuation coefficient of a standard atmosphere at ground level to the linear attenuation coefficient of water.

The attenuation of the signal by the aluminum tubing around the detector will vary according to the position

of the target area on the cylinder (sidewall or bottom). We also have to account for the dispersion in space of the gamma rays and the surface of the target area orthogonal to the trajectory of the gammas. For a source located a θ with respect to the vertical axis of the crystal, the response of the crystal (R) or its ability to capture the totality of the energy of incoming gammas is given by

$$R(\theta) = E \sum_{i=1}^{n} [(1 - e^{-\beta_{\mathrm{NaI}} T_i})(1 - X_i)], \qquad (3)$$

where E is the efficiency of the photomultiplier and electronics of CS725 to properly detect the gammas absorbed by the crystal; n, where $i = 1, \ldots, n$ is the number of target areas on the surface of the crystal; β_{NaI} is the linear attenuation coefficient of the detector (NaI); T_i is the length of the trajectory of a gamma nonattenuated through the crystal; and X is the proportion of the gammas exiting the crystal after one or more collisions with an electron of the crystal.

The linear attenuation coefficient of a NaI crystal is relatively high (more than 3 times that of water for the energy windows of interest); it is such that some 15% of the 1.46- and 2.61-MeV gammas suffer a collision within the first centimeter of their trajectories (T_i) in the crystal. At these energy levels, Compton scattering predominates over photoelectric absorption and pair production (Gilmore 2008). When the gamma is not totally absorbed, its energy is reduced, therefore increasing the probability of subsequent Compton scattering or photoelectric absorption. For this reason, we consider the factor X in Eq. (3) to be significantly smaller than one. After a Compton collision between a gamma and a free electron, the trajectory of the resulting gamma is different. The trajectory varies from case to case. We assume that it could go in any direction (Gilmore 2008). We therefore consider that $(1 - X_i)$ varies little for different values of i, or different target areas being located at the center or peripheral of the crystal. We use the hypothesis that the term $(1 - X_i)$ in Eq. (3) can be statistically replaced by a constant that has a value close to one. The resulting hypothesis is that, for a large population of gammas, the response of the detector to incoming gammas is approximately the following:

$$R(\theta) \propto \mathrm{Const.} \times \sum_{i=1}^{n} (1 - e^{-\beta T_i}). \qquad (4)$$

A number of simulations were conducted to select the optimal values for the different parameters defining the resolution of the model: n, C, D, and S. We progressively increased in our simulations the value of these parameters until we noticed only very marginal changes to the results. For example, with the parameter S, the number of layers of soil, we doubled the number from 25 to 50 and simulated the response N/N_o of the CS725. For an SWE of 20 cm, N/N_o increased from a value of 0.2141 to 0.2142. This translates to an error of less than 0.1 mm of SWE. We therefore set the value of S to 25. Each layer has a depth of 1.6 cm for a total depth of 40 cm. Vertical concentric cylinders C is set to a value of 25 covering a range of θ from 0° to 87.3°. Increasing the value of the parameter C from 25 to 80 results in less than 1-mm difference on SWE estimates. The vertical surface of the detector is divided into 60 layers while, because of the symmetry of the setup, we target only one of the horizontal halves of the detector and divide it into 30 columns for a total of 1800 target areas. Finally, the model allows for different vertical distributions of the soil parameters: density, water content, and emissivity. The selected vertical distribution is common to all of the annular sections.

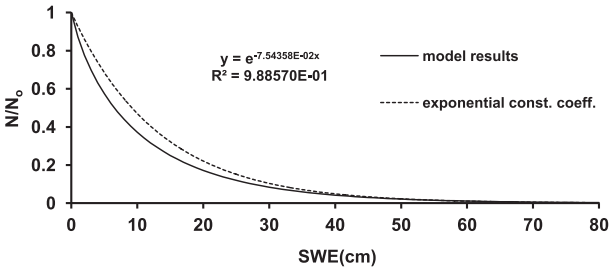

FIG. 3. As derived from the model N/N_o against SWE and an exponential function with a constant attenuation coefficient.

3. Snow water equivalent

Because of the proportional nature of Eq. (4) and the fact that the total effective radiation is site specific and unknown beforehand, a calibration procedure is conducted at each new site. This procedure will be briefly described in section 5.

Based on the simulation results, we looked for a relation between the signal registered by the CS725 and SWE. Using the least squares technique, we selected an exponential of the form given in Eq. (4) as the most appropriate. This is the type of function [Eq. (5)] used so far to extract SWE measurements from data collected by airborne gamma detectors:

$$N \propto e^{(-\alpha \mathrm{SWE})}, \qquad (5)$$

where N is the counts of gammas detected and α is the exponential coefficient.

In Fig. 3, we present the results of the numerical simulations (dotted line) over a totally dry soil for varying values of SWE. The counts for the different

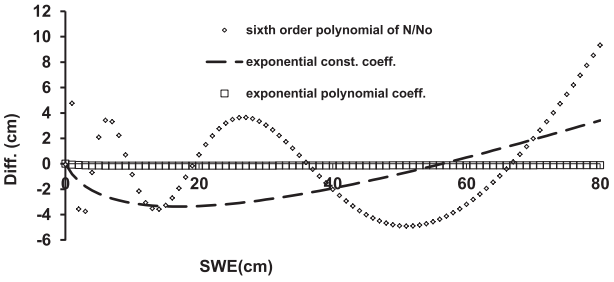

FIG. 4. Performances of three types of functions between N/N_o and SWE.

values of SWE are plotted as ratios to the counts (N_o) detected in absence of a snow cover and soil moisture. An exponential of the type of Eq. (5), with a constant coefficient, appears to be approximately right. But while conducting some simulations involving limited source areas, we noticed that shrinking the source area (soil surface) impacts the value of the coefficient for a given SWE value. On the other hand, as the snowpack builds up, because of their slant trajectories, gamma rays incoming from peripheral source areas are more severely attenuated than their counterparts, closer to the center of the monitored area. The effective source area shrinks as the snowpack builds up, which led us to the concept of a variable coefficient function of SWE. Out of the simulation results, we therefore established a table of coefficients against SWE and identified (using the least squares technique) a sixth-degree polynomial to replace the constant coefficient. We obtain

$$N/N_o = e^{(-\alpha_{\mathrm{SWE}}\mathrm{SWE})}, \tag{6}$$

where α_{SWE} is the sixth-degree polynomial function of SWE.

In Fig. 4 we present the performances of three types of functions between N/N_o and SWE. We see that the exponential-type function with a polynomial as a coefficient fits closely with the simulation results.

In practice, when analyzing the raw data from the CS725, we use an iterative process to derive an estimate of SWE. It consists of calculating an SWE value using a coefficient corresponding to the last SWE value reported by the CS725 at the site. This new value of SWE is used to establish a revised value to the coefficient, leading to a modified value of SWE. The process is repeated until the value of SWE converges (variations less than 1 mm). Only two or three iterations are normally required.

The target area monitored by the CS725 is quite large. In the absence of a snow cover on the ground, some 90% of the signal captured by the CS725 originates from a target area enclosed within 10 m of the sensor hung up

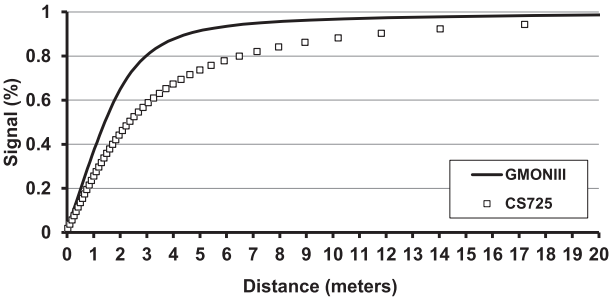

FIG. 5. Proportion of the signal originating from within X meters of the vertical axis of a GMONIII and a CS725 in the absence of snow.

at 2.5 m above ground (see Fig. 5). In the case of the shielded CS725 (labeled as GMONIII in the figure), more than 95% of the signal is captured within the same distance. This main target area progressively shrinks as the snowpack builds up.

As indicated in Fig. 3, at higher values of SWE, large variations in SWE result in small variations in counts. Also, given the statistical nature of the radioactive processes, one would want to handle high count numbers, so as to minimize statistical noise in the data. Therefore, the measuring period was extended to 24 h and programmed in the firmware of the CS725. Observations are available at 6-h intervals, so as to be synchronized with the World Meteorological Organization synoptic observation program. Each observation covers the previous 24-h period.

The possibility of using a larger NaI(Tl) crystal for the detector is another option. According to our simulations, using a cylindrical crystal of 10.2 cm × 12.7 cm instead of the current 7.62 cm × 7.62 cm detector would increase the number of counts by a factor of 3.5 (Fig. 6). Also, the variations in counts for each increment of SWE are higher for the large detector. For example, with the soil water content set at 30%, the variation of counts between values of 30 and 35 cm of SWE in the case of a 7.62-cm detector is similar to

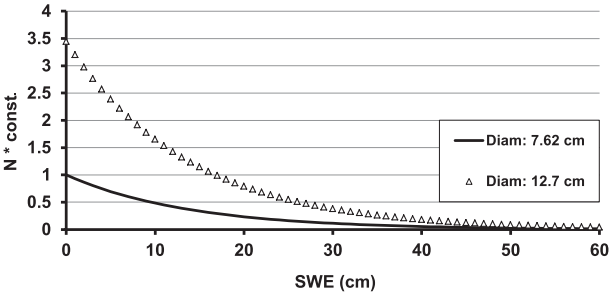

FIG. 6. Relative variations in counts in SWE for both the 7.62- and the 12.7-cm detectors $-M = 30\%$.

TABLE 2. Comparison of CS725 observations with snow pit measurements.

Year	No. of samples	SWE range (mm)	STD (%)
2012	7	119–222	5
2013	6	175–225	4

the variation observed between 47 and 52 cm by the large detector. This is an indication of the enhanced sensitivity of the 12.7-cm detector and the possibility of adapting the CS725 to cover a larger range of SWE.

Snow core and snow pit techniques were used as reference benchmarks. In the case of the snow core technique, one collects vertical samples at different points in the snowpack using a hollow tube to estimate the depth and density of the snowpack. The more reliable snow pit technique consists of digging pits and collecting information on each layer of snow, ice, or wet snow. In Table 2 a comparison is presented between the CS725 estimated values for SWE and snow pit measurements at different sites in operation in 2012 and 2013 (the number of samples stands for the number of reference measurements on the sites using the snow pit technique and STD stands for standard deviation between the SWE reported by CS725 and the benchmark measurements). These results are an indication of the reliability and accuracy of the CS725 and the capability of the model to reproduce the response of the instrument.

4. Soil moisture

Soil moisture content is a key factor in the calibration process of a CS725 site, as it does significantly attenuate the signal emitted by the ground. The relation between CS725 counts and SWE shown in Fig. 3 is only valid for totally dry soils, with zero moisture content. According to the literature, the effect of soil moisture content is driven by Eq. (7) below (Maxson et al. 1996; Fritzsche 1982). The factor F is set to a value of 1.11, which is the ratio of the electronic cross section of soil to the cross section of water:

$$N = N_o/(1 + FM), \tag{7}$$

where N is the counts of gamma detected, M is the soil moisture content expressed as a mass of water over the mass of dry soil per unit volume, and N_o is the N in absence of a snow or water cover and over a totally dry soil.

The value of 1.11 for F is reproduced by the model (Fig. 7). The range of simulations extends from 0% to 70% moisture content. It is useful to get some insight

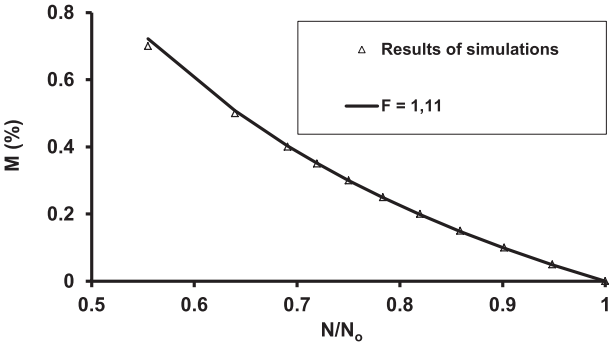

FIG. 7. Soil moisture content vs N/N_o as per the model.

into the meaning of M as reported by the CS725. How is the instrument reacting to vertical variations in soil moisture? From the numerical simulations, we understand that the water content of the very top layer of soil is the driving factor (Fig. 8). The top layer containing the first 25 g of homogenous dry soil per square centimeter is the source of more than 90% of the signal detected by the CS725. The fact that the signal measured comes from the very top layer of soil has been reported before (Fritzsche 1982). Furthermore, we conducted simulations initializing the model with various vertical distributions of moisture and did arrive at one overall conclusion: the CS725 is essentially measuring soil moisture content of the very top layer of soil with little consideration for moisture content at deeper levels in the ground. For a typical dry soil density of 1.6 g cm^{-3}, this represents the top 15 cm of soil. Even if the ground is soaked with water underneath a relatively dry top layer, the CS725 reports a value of M that is very close to the moisture content of the top soil layer. The reverse is also true.

For equal values of M, the depth of this significant top layer of soil will increase, as demonstrated by the model, when the soil is of a more organic type and therefore presents a lower density when dried out.

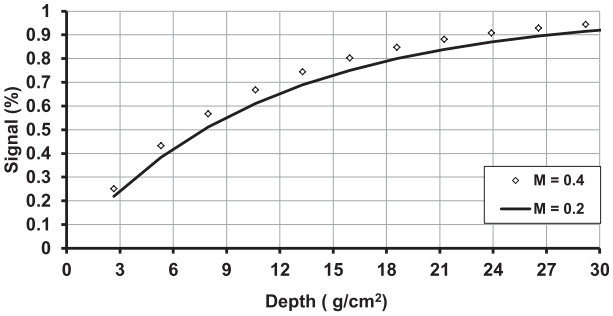

FIG. 8. Percentage of the total signal originating from the top layer of soil vs its depth expressed in g cm^{-2}.

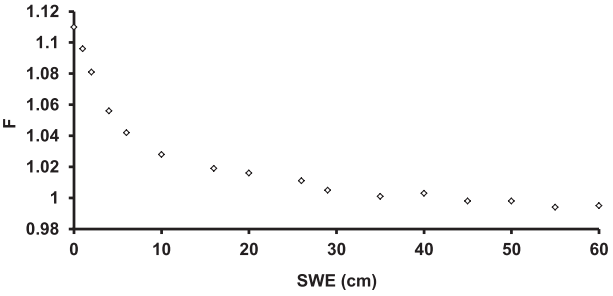

FIG. 9. The F factor vs SWE.

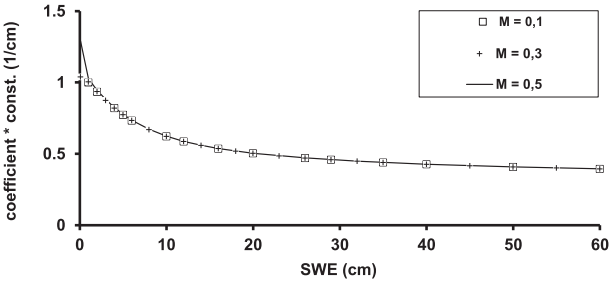

FIG. 11. Effective attenuation coefficients for different M and SWE values.

5. Snowpack and soil moisture

As a result of all of this, Eq. (8) is used for interpreting the data registered by the CS725:

$$N/N_o = 1/(1 + FM)\, e^{(-\alpha_{\mathrm{SWE}}\mathrm{SWE}left)} \qquad (8)$$

Furthermore, the analysis of results gathered from the numerical simulations raises an interesting particularity: the response of the detector to variations in M is different for different SWE values. The F factor in Eq. (8) varies with SWE. Apparently, the well-known 1.11 factor applies only to situations with no snow cover on the ground.

Figure 9 shows the values of F for different values of SWE. One notices that, for higher values of SWE, F remains relatively constant at a value close to one. The larger variations are for SWE values between 0 and 10 cm.

In retrospect, this is not surprising because we have noted, from numerical simulations, that the F factor gets down to a value of 0.95 when we restrict the source area to within an angle of 10° with the vertical axis of the detector. The presence of a snowpack produces a similar effect of reducing the effective source area by attenuating more severely the gammas originating from the peripheral areas. This is again due to the slant trajectory of these gammas through the snowpack.

Using a constant F value of 1.11 in Eq. (8) instead of a function of SWE leads to errors on SWE. The resulting errors are described in Fig. 10. They are larger for higher values of M but are still quite small, in the order of a few millimeters in the worse cases (high M associated with high SWE values).

We also note from the outputs of the model that the effective attenuation coefficient varies slightly with M. But the variations are so small (Fig. 11) that they do not impact significantly on the values of SWE derived from the CS725's data. These small differences in SWE, on the order of 0.1 mm, might also be an approximation error by the model given its limited resolution.

In winter, to derive SWE from Eq. (8), one needs to estimate beforehand the value of M. One could think of soil core sampling, although this is not easy when the soil is frozen. To bypass the difficulty of measuring M in winter, we estimated the winter value of M from field measurements made late in fall.

To support this, we show in Fig. 12 the errors resulting from a wrong estimate of M instead of, in this case, a real value of 0.3. A value of M dryer than the real value conducts to an overestimate of SWE. An error of the order of 0.2 on M introduces an error of some 2 cm on a snowpack SWE of 60 cm.

But in order to use effectively Eq. (8), one has to estimate N_o. This parameter is site specific. It is the

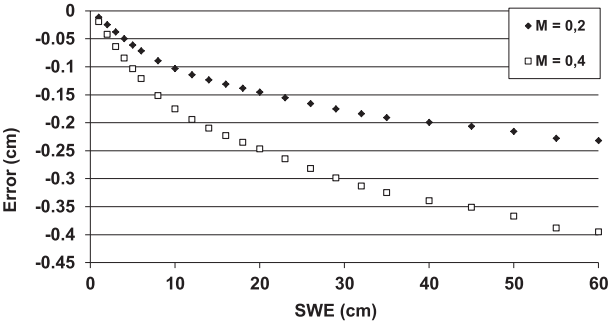

FIG. 10. Errors resulting from keeping F constant at 1.11 instead of varying F with SWE.

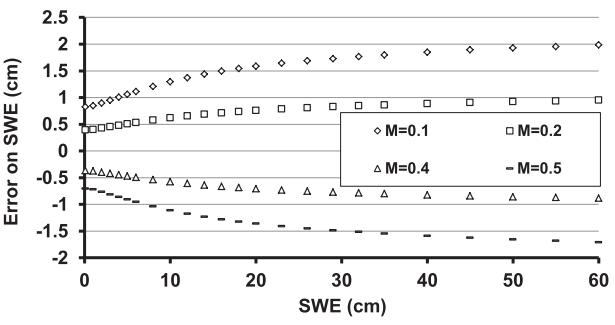

FIG. 12. Errors on SWE estimates when M differs from the real field value ($M = 0.3$).

number of counts that would be reported by the CS725 in absence of a snow cover and over a totally dry soil. An initial value for N_o is calculated from Eq. (8) with SWE set at zero and M set at the estimated or preferably measured value of soil moisture content. This procedure applies in absence of a snow cover.

6. Conclusions

Numerical modeling has been of great assistance with the development of CS725. We simulated its behavior and extracted out of the simulations the data interpretation algorithms to estimate SWE with an accuracy of 5%. The simulation model is based on a few key factors. Stripping of the counts to isolate the 1.46- and 2.61-MeV gammas allows for a monochromatic approach to modeling. Also, instead of using a Monte Carlo technique to simulate the absorption of gammas by the detector [crystal of NaI(Tl)], we worked out a simple model based on the assumptions that once collided with an electron, the resulting attenuated gamma stand little probability of getting out of the crystal (total absorption therefore recognized and counted by the CS725) and that this probability can be considered as constant for whatever the point of entry on the crystal.

According to the results of the simulations, we found that SWE impacts on the size of the area, effectively monitored by the instrument and therefore on the algorithm to be used to translate counts by the CS725 in SWE values. An exponential function of SWE with a coefficient, itself a sixth-degree polynomial function of SWE, was identified as a reliable and accurate mathematical relation between the counts and SWE over the area monitored. The size of the area effectively monitored by the CS725 extends to 10 m from the detector when there is no snow or water on the ground. The size of the area decreases with increasing SWE.

The top 25-g layer of soil is the source of 90% of the signal detected by the CS725, and the moisture content of this layer is essentially the moisture content detected by the instrument with little contribution of the moisture contents from deeper layers.

We also reproduced the relation between the signal and soil moisture content identified by Fritzsche (1982) and the 1.11 coefficient for application over a ground surface in absence of a snowpack or of a layer of water above ground.

REFERENCES

Carroll, T. R., and J. C. Schaake Jr., 1983: Airborne snow water equivalent and soil moisture measurement using natural terrestrial gamma radiation. *Optical Engineering for Cold Environments,* G. W. Aitken, Ed., International Society for Optical Engineering (SPIE Proceedings, Vol. 0414), 208, doi:10.1117/12.935888.

Choquette, Y., P. Lavigne, P. Ducharme, A. Houdayer, and J.-P. Martin, 2008: Apparatus and method for monitoring snow water equivalent and soil moisture content using natural gamma radiation. US Patent 7,800,051, filed 9 January 2008, and issued 21 September 2010.

Fritzsche, A. E., 1982: National Weather Service gamma snow system physics and calibration. NWS Publ. NWS-8201, 37 pp.

Gilmore, G., 2008: *Practical Gamma-Ray Spectrometry*. 2nd ed. John Wiley & Sons, 408 pp.

Grasty, R. L., 1982: Direct snow-water equivalent measurement by air-borne gamma-ray spectrometry. *J. Hydrol.,* **55,** 213–235, doi:10.1016/0022-1694(82)90131-7.

Martin, J.-P., A. Houdayer, C. Lebel, Y. Choquette, P. Lavigne, and P. Ducharme, 2008: An unattended gamma monitor for the determination of snow water equivalent (SWE) using the natural ground gamma radiation. *2008 IEEE Nuclear Science Symposium and Medical Conference,* P. Sellin, Ed., IEEE, 983–988.

Maxson, R. W., T. R. Carroll, and A. A. El Haddi, 1996: Airborne measurement of snow water equivalent and soil moisture. *Proceedings of the Second International Airborne Remote Sensing Conference and Exhibition: Technology, Measurement and Analysis*, Vol. 2, Environmental Research Institute of Michigan, II-492–II-500.

National Institute of Standards and Technology, cited 2013: XCOM: Photon cross sections database. [Available online at http://www.nist.gov/pml/data/xcom/.]

Offenbacher, E. L., and S. C. Colbeck, 1991: Remote sensing of snow covers using the gamma-ray technique. U.S. Army Corps of Engineers Cold Regions Research and Engineering Laboratory CRREL Rep. 91-9, 26 pp.